Natural Hazards (2026) 122:311
https://doi.org/10.1007/s11069-026-08071-3

ORIGINAL PAPER

Multidisciplinary monitoring of mud volcanoes: a new perspective on fluids and seismicity link from the Salse di Nirano (Italy)

E. Ferrari[1] · A. L. Rizzo[1,2] · G. Capelli Ghioldi[3] · A. Sciarra[4] · G. Tamburello[3] · F. Viveiros[5] · S. Lovati[1] · M. Massa[1]

Received: 1 October 2025 / Accepted: 20 February 2026

Abstract
Understanding the relationship between fluids and seismicity is crucial for improving seismic hazard assessment, as fluid migration can play a significant role in earthquake triggering. Here, we present the results from an innovative real-time multiparametric monitoring implemented at the so-called 'Salse di Nirano' or mud volcano field (Northern Apennines, Italy), a region of medium to high seismic hazard. The objective is to investigate how geofluid dynamics relate to local seismicity. Two bubbling mud pools were selected for continuous monitoring of mud level, temperature, and electrical conductivity. Additionally, a CO_2 flux station was installed on the field's edge, where elevated gas emissions are observed. Complementary meteorological and seismic stations track atmospheric conditions and seismic activity. Notably, anomalous shifts in mud pool electrical conductivity and soil CO_2 flux were recorded in temporal correlation with two distinct seismic swarms in 2024, highlighting the potential of fluid-geochemistry monitoring as a tool for tracking subsurface processes linked to seismic unrest.

Keywords Crustal fluids · Pre-seismic anomalies · Multiparametric stations · Mud volcano hazard

✉ E. Ferrari
elisa.ferrari@ingv.it

1 Istituto Nazionale di Geofisica e Vulcanologia (INGV), Milan, Italy

2 Department of Earth and Environmental Sciences, University of Milano-Bicocca, Milan, Italy

3 Istituto Nazionale di Geofisica e Vulcanologia (INGV), Bologna, Italy

4 Istituto Nazionale di Geofisica e Vulcanologia (INGV), Roma 1, Italy

5 Instituto de Vulcanologia e Avaliação de Riscos, Universidade dos Açores, Ponta Delgada, Portugal

Published online: 13 March 2026

1 Introduction

Mud volcanoes are natural surface expressions of fluids originating from deep within the Earth's crust, including methane, carbon dioxide, saline water, sediments, and occasionally oil. They occur worldwide across all tectonic settings and are typically associated with diagenetic or catagenetic hydrocarbon generation systems (Mazzini and Etiope 2017). Methane of microbial or thermogenic origin generally dominates their gas emissions, followed by CO_2 and nitrogen (Etiope and Martinelli 2009; Etiope 2015). The main driving forces of this focused fluid flow are gravitational instability in fine-grained sedimentary rocks and gas overpressure, but other complex processes also play key roles, including the presence of pre-existing fractures, changes in the local stress regime, and earthquake activity (Mellors et al. 2007; Manga et al. 2009; Mazzini and Etiope 2017).

Understanding the complex dynamics of mud volcanoes, especially their relationship to tectonic and seismic activity, requires continuous and high-resolution monitoring. While many studies have focused on discrete sampling of gases and fluids to investigate their chemical and isotopic compositions (Etiope et al. 2004a, b; Yang et al. 2004; Baciu et al. 2007; Chao et al. 2010; Etiope et al. 2011; Queißer et al. 2017; Chen et al. 2019; Sciarra et al. 2019), fewer works have addressed continuous long-term monitoring of physical parameters such as the mud level, fluid temperature, and gas fluxes (Martinelli and Dadomo 2005, 2017; Kopf et al. 2010; Delisle et al. 2011). Some studies have measured temperature profiles inside mud conduits, particularly in submarine systems (Kaul et al. 2006; Feseker et al. 2008, 2009, 2014), but long-term datasets combining gas and seismic data remain scarce. Notably, there is a clear lack of continuous, high-frequency monitoring of soil gas emissions in direct relation to seismicity in the existing literature.

The present study addresses this gap by reporting the first results of a long-term, multiparametric monitoring at the Salse di Nirano mud volcano field (Modena Province, Northern Italy). This site is known for persistent, non-eruptive activity and has been the focus of only two previous continuous studies: (i) Martinelli and Dadomo (2017), who monitored the mud level and temperature over a 10-month period at 10-minute intervals, and highlighted that geochemical and hydrogeological precursors to earthquakes are structurally controlled by deep features and preferential fluid migration pathways; and (ii) Giambastiani et al. (2022), who conducted four months of monitoring on the mud level, temperature, and specific electrical conductivity (EC) across four structures, with a 5-minute sampling rate. Their work demonstrated that CO_2 and CH_4 fluxes at Nirano are strongly influenced by steeply dipping faults that serve as conduits for deep gas migration. The presence of flux anomalies aligned with fault structures confirms the importance of tectonic control on fluid dynamics in mud volcano systems.

The monitoring system implemented in this study stands out for its duration (~19 months), multiparametric nature (including three mud-related parameters, soil CO_2 fluxes, seismic signals, and meteorological data), and spatial coverage of three distinct areas within the Nirano field (two mud pools—La Giunta and F—and one site for soil CO_2 flux). Geochemical data are acquired at a high temporal resolution (up to 1 datum per minute), which is unprecedented for this area. Moreover, this is the first long-term continuous dataset on soil CO_2 emissions from Nirano. By integrating geochemical, geophysical, and environmental datasets, this study contributes to our understanding of how fluids migrate through mud volcano systems and how such processes may be linked to local seismicity. In doing so,

it contributes to the broader effort of evaluating the role of fluid overpressure and migration in modulating seismic hazards in tectonically active sedimentary basins. Nirano site is part of the network of multiparametric stations described by Ferrari et al. (2024). Data are stored in the MUDA-DB (geophysical and geochemical MUltiparametric DAtabase; Massa et al. 2024) and they are open to free access at https://muda.mi.ingv.it.

2 Geological, seismotectonic and geochemical framework

The Nirano mud volcano field belongs to a cluster of ~20 mud volcanoes scattered across the Emilia-Romagna region (Castaldini and Coratza 2017). These features align along the Pede-Apennine margin of the Northern Apennines, a NE-verging fold-and-thrust belt (Fig. 1a). The area is seismically active due to regional tectonics associated with the Apennine thrust fronts and is classified as having medium to high seismic hazard (MPS Working Group 2004; Stucchi et al. 2011). The most significant historical earthquake close to Nirano occurred on June 5, 1501 (Mw 6.05; Rovida et al. 2020); in the last 40 years the INGV instrumental bulletin (https://terremoti.ingv.it/) only shows a moderate event of Md 4.1 that occurred close to Nirano (~10 km) on June 19, 2002 (focal depth of 19 km), even if the area was strongly hit by the 2012 Emilia sequence, Mw 6.1 (Luzi et al. 2013), occurring ~50 km NE from Nirano.

Nirano volcanoes develop within the Plio-Pleistocene Argille Azzurre Formation, consisting mainly of marly-silty clays (Gasperi et al. 2005). They are located in an ellipti-

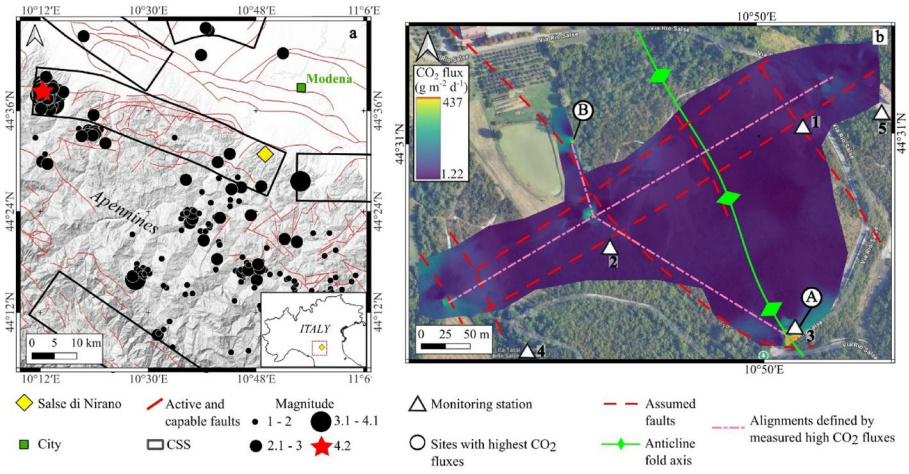

Fig. 1 **a** Simplified map of the surroundings of Salse di Nirano. The Coordinate System is WGS 1984, EPSG 4326. DTM 0.5 × 0.5 m from https://geoportale.regione.emilia-romagna.it/catalogo/dati-cartografici/altimetria/layer-5 is used as background layer. Magnitude of year 2024 earthquakes (INGV bulletin) are reported. Active and capable faults are taken from the ITHACA database (https://sgi.isprambiente.it/ithaca/viewer/index.html; ITHACA working Group 2019). Composite Seismogenic Sources (CSS) are taken from the Database of Individual Seismogenic Sources (http://diss.ingv.it). (**b**) Google Earth satellite image of the Salse di Nirano area. Monitoring stations are: (1) Probe inside La Giunta mud pool; (2) Probe inside F mud pool; (3) Permanent soil CO_2 flux station; (4) Permanent seismic station; (5) Meteorological station. Soil CO_2 flux map obtained from July 2023 measurements is shown. Assumed faults and anticline fold axis are redrawn after Castaldini et al. (2005, 2017), Bonini (2007)

cal depression along an anticline ridge with typical NW–SE Apennine orientation (Bonini 2012; Fig. 1b). This depression has been interpreted either as a mud volcano caldera formed by progressive collapse due to degassing (e.g. Bonini 2008) or as the final stage of mud diapir evolution (Castaldini et al. 2005).

Gas emissions are dominated by CH_4 (~98%), with minor components of CO_2, N_2, C_2–C_{10} hydrocarbons, and noble gases (Minissale et al. 2000; Etiope et al. 2007; Tassi et al. 2012; Sciarra et al. 2019). Isotopic analyses (δ^{13}C-CH_4 and δD-CH_4) suggest a primarily thermogenic origin, with secondary microbial CO_2 and some biodegradation (Heller et al. 2011; Sciarra et al. 2019). The liquid phase is mostly brackish connate water from the Argille Azzurre Formation (Minissale et al. 2000; Cipriani et al. 2017) and potentially the deeper Marnoso Arenacea Formation (Bonini 2012). Fluid migration is facilitated by thrust faults and fractures (Gorgoni et al. 1988; Giambastiani et al. 2022). The fluid composition, including dissolved ^{222}Rn, provides insights into the interplay between tectonics and degassing (Gorgoni et al. 1988; Martinelli et al. 1995). Historical and geochemical studies (Coppi 1875; Martinelli and Ferrari 1991; Bonini 2009) confirm that mud volcano activity in this area is closely linked to tectonic processes.

3 Materials and methods

A continuous, long-term multiparametric monitoring system has been established at the Salse di Nirano site, targeting two mud pools (La Giunta and F; monitoring began on April 24, 2023), one soil CO_2 flux site (from September 26, 2023), seismic signals (from June 23, 2023), and meteorological parameters (from June 6, 2023). Data reported in this study are up to mid November 2024.

At La Giunta mud pool (Figs. 1b and S1a), the mud level, specific electrical conductivity (EC), and temperature are measured with a CTD-Diver® (Van Essen Instruments, https://www.vanessen.com/) deployed at a depth of ~8.5 m. The mud level is recorded as the height of the column above the diver, using a piezoresistive ceramic sensor that also take atmospheric pressure into account (accuracy ± 0.5 cm, resolution 0.2 cm). A modem (GDTS, Royal Eijkelkamp, https://www.royaleijkelkamp.com/) provides atmospheric pressure data for barometric compensation. EC is measured with a four-platinum electrode cell (accuracy ± 1%, resolution 0.1%), and temperature with a semiconductor sensor (accuracy ± 0.1 °C, resolution 0.01 °C). The diver collects data at 1-minute intervals, which are transmitted daily to the INGV acquisition center via the Eijkelkamp server. To verify diver placement and assess mud column changes, vertical profiles of temperature and conductivity were recorded at 1 m/min with measurements every 2 s.

At F mud pool (Figs. 1b and S1b), monitoring is conducted using an STS multiparameter probe (https://www.sts-italia.it/) installed at ~1 m depth. The device includes a pressure sensor (precision 0.05% full-scale), a temperature sensor (accuracy ± 0.1 °C), and a 6-electrode titanium conductivity sensor (error < 2.5% of range). Initially set to a 10-minute sampling rate, the interval was extended to 1 h due to transmission issues. Data are transmitted daily via modem and forwarded to INGV by server-to-server transfer. A vertical profile was also performed here to compare with La Giunta.

Pressure sensors of both probes (CTD-Diver and STS) return a pressure value expressed in mH_2O, which is then automatically converted in the water level considering water density

(1000 g/L). Since mud density is greater than that of water (1247 g/L reported by Giambastiani et al. 2022 for Nirano mud samples), the level readings are overestimated by ~1 m.

In July 2023, a soil gas survey was conducted to identify a site for permanent CO_2 flux monitoring. A portable flux station (Thearen, https://thearen.com/) using the accumulation chamber method (e.g. Chiodini et al. 1998) was employed. CO_2 concentrations (0–2 vol%) were measured with a LICOR infrared analyzer (LI830-3). A total of 126 measurements were taken across vegetated and clay-dominated areas under stable weather. Spacing was 40 m, reduced to 5–10 m in areas of high flux. Measurements lasted 1–1.5 min, with corrections applied for temperature and pressure inside the chamber. Data were interpolated using Inverse Distance Weighting (IDW) to create a flux distribution map. Gas samples were collected at sites with peak fluxes for further analysis. The $\delta^{13}C–CO_2$ and $\delta^{13}C–CH_4$ values (expressed in ‰ relative to V-PDB) were analyzed using the Cavity Ring-Down Spectroscopy (CRDS) technique (G2201-i, Picarro, Santa Clara, CA, USA) at INGV Rome1, Italy. The operating range was 380–2000 ppm for CO_2 and 1.8–4,000 ppm for CH_4 (simultaneous precision mode). Measurement precision was better than 0.16‰ for $\delta^{13}C–CO_2$, and better than 1.15‰ in high-precision mode and 0.55‰ in high dynamic range mode for $\delta^{13}C–CH_4$.

A permanent Thearen station for CO_2 soil flux measurements was then installed at location A (Figs. 1b and S1c), where elevated CH_4 and CO_2 fluxes were identified. Monitoring focused on CO_2, considered more sensitive to feeding system variations due to its lower concentration compared to CH_4. The station uses a non-stationary flux chamber and a LICOR analyzer (LI830-3; 0–2 vol%), with hourly measurements (3-minute intervals), corrected for chamber temperature and pressure. Soil temperature (Pt100, ± 0.5 °C), soil moisture (CS616, ± 2.5 VWC), and meteorological variables (atmospheric pressure, temperature, humidity, rainfall, wind speed and direction) are simultaneously recorded. Data are sent daily to the company's cloud server and then to INGV via a dedicated router.

To determine the CO_2 background flux, the Graphical Statistical Analysis (GSA; Sinclair 1974; Chiodini et al. 1998) was applied to both the soil gas survey and the permanent station datasets. Lognormal populations were identified using probability plots, and the background threshold was set at the 95th percentile.

The Davis Vantage Vue® weather station (Figs. 1b and S1d; https://www.davisinstruments.com/) collects meteorological data at 1-minute intervals, which are logged by the WeatherLink Live™ console and transmitted via API to INGV. In case of missing data, information from nearby ARPA Emilia-Romagna Dext3r stations (https://simc.arpae.it/dext3r/) is used.

On June 6, 2023, a short-period seismic station was installed near the La Giunta pool (Fig. S1e) to monitor bubble emission rates, frequency content, and potential correlations with seismic events. The setup included a Reftek-130 24-bit datalogger (https://reftek.com/) and two Lennartz 5s seismometers (https://www.lennartz.de/en/), sampling at 100 and 200 Hz, respectively, over an 8-hour daytime period without wind. Seismometers were covered and partially buried to reduce noise. On June 23, 2023, a permanent station (ZO.PDN10, https://doi.org/10.13127/sd/yhcfomcbo_), part of the PDnet network (Ferrari et al. 2024), was installed ~ 360 m from La Giunta and ~ 240 m from F. It uses a Gaia2 system (Rao et al. 2010) and a Lennartz 5s seismometer sampled at 100 Hz. Data are streamed in real-time to INGV Milano and are accessible via the European Integrated Data Archive (EIDA; https://eida.ingv.it/en/) (Danecek et al. 2021). The data processing follows the scheme proposed in Massa et al. (2024) including the daily data download of 24 h miniSEED file, its separation

into 288 sub-windows, each one with length of 5 min, the removal of the sensor response curves by deconvolution, the conversion of raw data in the proper physical unit (i.e. cm/s) and finally the application of a 4th order Butterworth filter in the range 0.1–40 Hz. For each single sub window, the RMS (Root Mean Square, e.g. Goldstein et al. 2003) and the FFT(f) (Fast Fourier Transform, e.g. Bormann 2012) for frequency interval from 0.1 Hz to 20 Hz, are calculated.

3.1 Time-series analysis

Python™ code (https://www.python.org/) was used to perform an initial assessment of the time-series completeness and to calculate basic statistical parameters, including minimum, maximum, mean, and standard deviation. The data were carefully screened to remove invalid values. For example, CO_2 flux values associated with $R^2 < 0.9$ were discarded. Time-series with missing data were reconstructed using linear interpolation. Additionally, the first derivative was calculated for the mud pool time-series to highlight short-term variations. The main Python libraries used for these tasks were Pandas, NumPy, and Matplotlib.

To identify cyclic behavior in the time-series signals, spectral analysis was performed using TSoft© software (https://seismology.be/en/downloads/tsoft; Van Camp and Vauterin 2005). Given that the time-series are shorter than two years, the analysis focused on daily and high-frequency periodicities, excluding seasonal and low-frequency components. Fast Fourier Transform (FFT) was applied, and Power Spectral Density (PSD) plots were evaluated. For the gas flux time-series, spectral changes over time were analyzed using a moving window spectrogram based on a Hanning window of 512 points and a step size of 24 samples (e.g. Oliveira et al. 2018).

SPSS® software (https://www.ibm.com/it-it/spss) was used to compute correlation coefficients among the different monitored parameters. Kendall's rank correlation was used for the mud pool datasets, which exhibited non-normal distributions, while Pearson's correlation was applied to the CO_2 flux data, which approximated a normal distribution. To evaluate the influence of environmental (meteorological and soil) parameters on CO_2 emissions, a stepwise Multivariate Regression Analysis (MRA) was conducted with CO_2 flux as the dependent variable. Initially, all environmental parameters were included as independent variables; subsequently, only those that met specific criteria were retained. Following the procedure outlined by Viveiros et al. (2015), variables were selected based on their Pearson correlation, significance in t-tests, contribution to an R^2 increase > 0.01, and reduction in the F index. Collinearity among independent variables was excluded, as Variance Inflation Factor (VIF) values remained below 10 (see Table S4). The resulting regression equation was used to compute predicted flux values and residuals (measured – predicted). These residuals were compared with earthquake events to investigate potential links between CO_2 flux anomalies and local seismicity. Although MRA could also be applied to mud pool parameters, due to their non-normal distribution, we instead used the first derivative of those time-series to assess potential earthquake-related variations.

4 Data and results

4.1 Mud column vertical profiles

Vertical profiles of temperature and electrical conductivity (EC) were acquired within the mud water columns of La Giunta and F mud pools (Fig. 1b and S1). Each vertical log was performed down to the maximum depth reachable in the respective mud volcano structure. La Giunta was found to be the deepest, with a depth of approximately 10.5 m (Fig. S2). Both mud pools exhibit increasing temperatures with depth, reaching comparable values at the bottom (~14 °C; Fig. S2). After an initial sharp increase near the surface, EC generally decreases slightly with depth or remains relatively constant, with values ranging between ~13,500 and 15,300 µS/cm (Fig. S1). A notable exception is the F mud pool, where EC shows significant oscillations in the upper few meters before stabilizing around 13,000 µS/cm at depth.

4.2 Continuous monitoring of La Giunta and F mud pools

Data on the mud water level, temperature, and EC collected between April 24, 2023, and November 15, 2024 are presented. Periods of data interruption or unreliable values are indicated by light grey boxes in Fig. 2. Labels A, B, C, and D refer to specific intervals during which La Giunta sensor depth remained unchanged despite the abovementioned disruptions. The longest uninterrupted monitoring period, referred to as interval D in Fig. 2, spans from November 9, 2023, to November 15, 2024. For the F mud pool, two periods of missing data occurred due to malfunctioning probe components.

Basic statistics for all three monitored parameters are summarized in Table S2. Both La Giunta and F mud pools exhibited substantial temporal variations in the mud water level, temperature, and EC, with some site-specific features. For instance, La Giunta recorded two temperature peaks of ~21.1 °C in August 2023, each accompanied by a slight increase in EC. EC trends are particularly noteworthy, especially given the rarity of high-frequency, long-term datasets of this kind in the literature. During interval D at La Giunta, three distinct phases were identified:

(i) an abrupt drop in EC (ΔEC ~ 230 µS/cm) at the end of February 2024, followed by a gradual decline (~25 cm) in the mud level during early March;
(ii) a phase of relatively stable conductivity from March to early July 2024;
(iii) a sharp increase in conductivity (ΔEC ~ 1140 µS/cm) in mid-July, which coincided with a significant rise (~30 cm) in the mud level and a slight decrease in temperature (ΔT ~ 0.5 °C).

At the F mud pool, EC remained stable around 11,700 µS/cm from April to September 2023, followed by a gradual decline. At the end of February 2024, a sudden increase was immediately followed by a dramatic drop (ΔEC ~ 6000 µS/cm), occurring just days before a similar decrease was observed at La Giunta. Conductivity at F then stabilized between March and July 2024 (~3000 µS/cm). Starting on July 22, values began fluctuating markedly, peaking at 16,487 µS/cm (Fig. 2), with this high variability subsiding by late October.

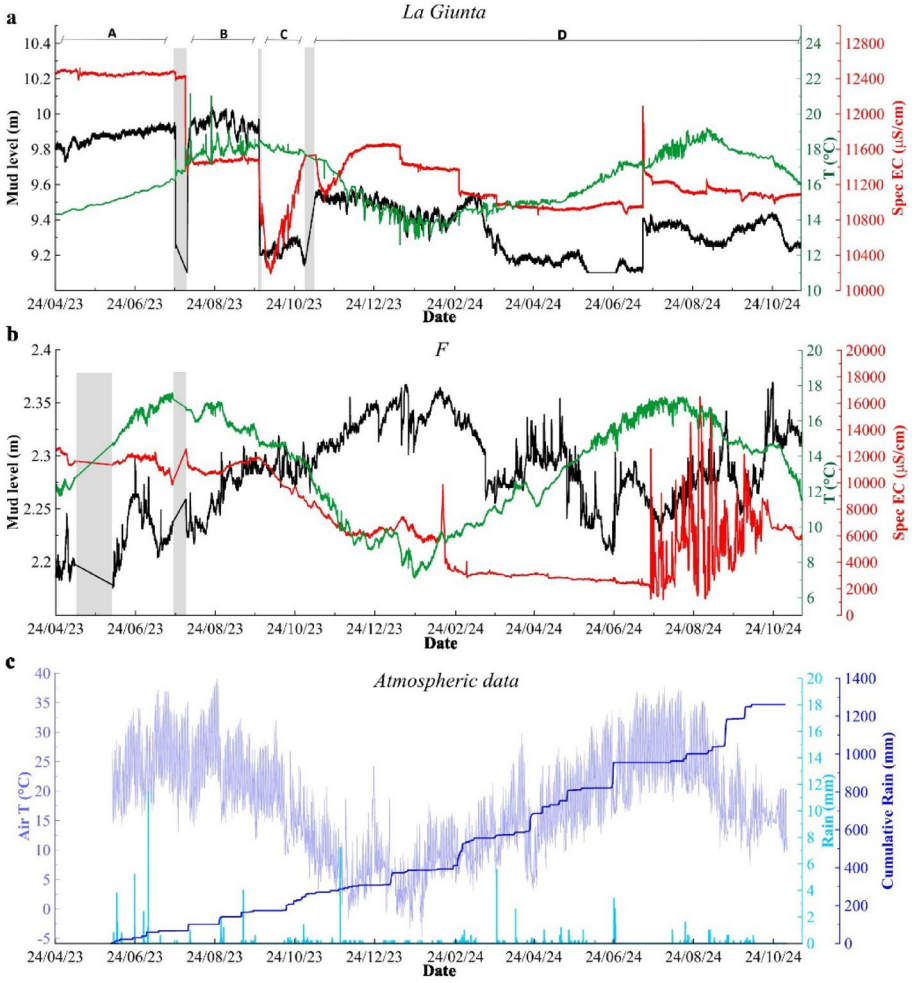

Fig. 2 Time-series of mud level (black), temperature (green) and specific EC (red) recorded at La Giunta (**a**) and F (**b**) mud pools. Light grey boxes represent time spans affected by data interruption or inconsistency. A, B, C, D represent self-consistent time spans data. (**c**) Atmospheric parameters: air temperature (light violet), rain (light blue) and cumulative rain (blue)

Mud water temperature at both sites follows a seasonal pattern, consistent with atmospheric temperature trends, as also reported by Mazzini and Etiope (2017). Correlation coefficients between mud and air temperature support this (La Giunta: 0.44; F: 0.64; Table S2). The slightly earlier temperature peaks at F are likely due to the shallower mud column (~2.3 m vs. ~9.5 m at La Giunta), which allows faster thermal equilibration with the atmosphere. Atmospheric pressure appears to have no meaningful effect on the mud level, as shown by low correlation coefficients (Table S2) and the absence of a linear relationship in barometric efficiency analyses (Fig. S2). In contrast, intense rain events often trigger sharp mud level decreases, likely due to dilution of the mud column, which sensors register as a pressure drop.

Kendall correlation coefficients between the two mud pools suggest a generally consistent behavior (Table S2), despite some site-specific differences. Daily oscillations and spikes in temperature and conductivity point to fluctuating mud fluxes, likely driven by mud and/or gas dynamics within the fracture system, as observed at other mud volcanoes (Deville and Guerlais 2009).

4.3 Spatial variability of soil CO_2 diffusive degassing

In July 2023, a soil CO_2 degassing survey was carried out in the Nirano area to select the optimal site for installing a permanent automatic station for continuous monitoring. CO_2 fluxes ranged from 1.22 to 437 g m^{-2} d^{-1} and were modelled following Sinclair (1974). Two overlapping lognormal populations were identified (Fig. S4a): Population A (65% of data) had a mean flux of 12.02 g m^{-2} d^{-1}, while Population B (35%) averaged 39.80 g m^{-2} d^{-1}.

Population A likely reflects biological CO_2 production, consistent with global background values between 0.2 and 21 g m^{-2} d^{-1} (Raich and Tufekcioglu 2000). Accordingly, the local biological background flux was defined as the 95th percentile of Population A (~28 g m^{-2} d^{-1}; Fig. S4a). Mud-covered areas showed fluxes near the biological minimum. Population B likely represents advective gas migration mechanisms and/or zones of higher permeability. Fluxes exceeding the background define two alignments (Fig. 1b): one NW–SE with the highest values (up to 437 g m^{-2} d^{-1}), and a second NE–SW trend with values up to 112 g m^{-2} d^{-1}. Anomalous emissions mostly occurred in unvegetated soils with mud cracks, indicating stress on vegetation.

Stable isotope analyses of CO_2 and CH_4 from high-flux sites (A and B in Fig. 1b) yielded $\delta^{13}C$–CO_2 values of −11.49‰ and −6.2‰, and $\delta^{13}C$–CH_4 of −39.07‰ and −52.24‰, respectively, indicating a thermogenic and secondary microbial origin, reflecting biodegradation processes that influence the carbon isotopic signatures of CH_4 and CO_2 (Fig. S4b), consistent with previous studies within the mud field (Tassi et al. 2012; Oppo et al. 2013; Sciarra et al. 2019).

4.4 Temporal variability of soil CO_2 diffuse flux

Thanks to the installation of a permanent soil flux station, temporal variability of soil CO_2 fluxes was investigated at location A (Fig. 1b), where the highest flux (437 g m^{-2} d^{-1}) was recorded during the soil gas survey. The time series presented here spans from September 27, 2023, to November 15, 2024 (Fig. 3a). CO_2 fluxes ranged from 0.97 to 204 g m^{-2} d^{-1}, with a mean value of 19.8 g m^{-2} d^{-1}. Data modelling, following the Sinclair (1974) method, revealed two overlapping lognormal populations: Population A (92% of the data) with a mean flux of 14.45 g m^{-2} d^{-1}, and Population B (8%) with a mean of 56.23 g m^{-2} d^{-1}. The background flux for the site was defined as the 95th percentile of Population A, corresponding to ~31.6 g m^{-2} d^{-1}. The highest values were recorded in early September 2024, following a period of sustained fluxes exceeding twice the average and above the background level since the previous month. The spectrogram (Fig. 3b) clearly shows a persistent diurnal cycle throughout the monitoring period, with additional higher-frequency components during July–September 2024, coinciding with elevated emissions.

Among environmental variables, only air temperature and humidity exhibited similar 1 cpd (cycles per day) periodicity (Fig. 3c, d). Soil temperature showed the closest correla-

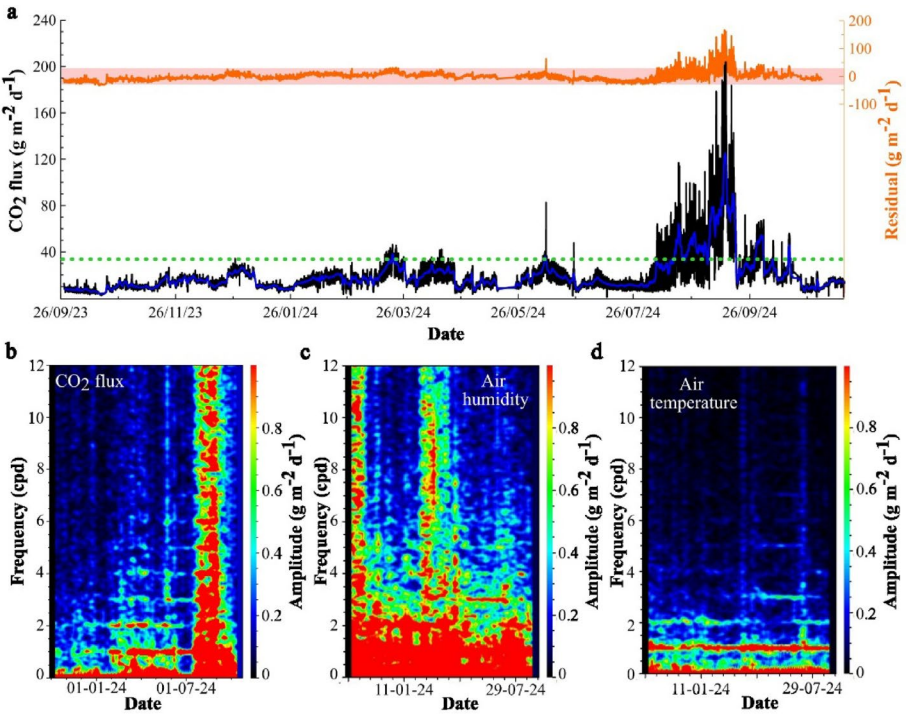

Fig. 3 **a** In black, the recorded CO_2 flux time-series. The blue line represents the running average of CO_2 flux calculated at 24 h. The dotted green line is the background flux recorded at the anomalous site where the permanent station is installed. In orange, residual of CO_2 flux calculated after multivariate regression analysis (see SI for details). The light red rectangle represents the $\pm 2\sigma$ interval. **b** Spectrogram of flux time-series data. **c** Spectrogram of air humidity time-series data. **d** Spectrogram of air temperature time-series data

tion with CO_2 fluxes (Pearson coefficient = 0.32; Table S2). Stepwise multivariate regression analysis identified soil temperature, soil humidity, and air temperature as the main explanatory variables, accounting for ~ 19% of the variance (Table S4). Their statistical significance was confirmed according to the t-test ($P < 0.01$; Table S4). Soil temperature contributed most significantly ($\Delta R^2 \approx 10\%$). Model reliability is supported by a correlation coefficient of 0.44 between measured and predicted flux values. Residual flux is shown in Fig. 3a.

4.5 Short-term and permanent seismic measurements

On June 6, 2023, a temporary seismic survey lasting approximately 8 h was conducted near the La Giunta mud pool to characterize the rate, amplitude, duration, and frequency content of high-frequency rhythmic "drumbeats" generated by bubble emissions. Over 3900 distinct events were identified during the recording period. The drumbeat signals typically lasted between 2 and 20 s, with dominant frequency content ranging from 5 to 30 Hz (Fig. S5) as already highlighted by Lupi et al. (2016) and Lucian et al. (2017).

To enable long-term monitoring of local seismicity and assess its correlation with other multidisciplinary time series, the permanent seismic station ZO.PDN10 (Ferrari et al. 2024)

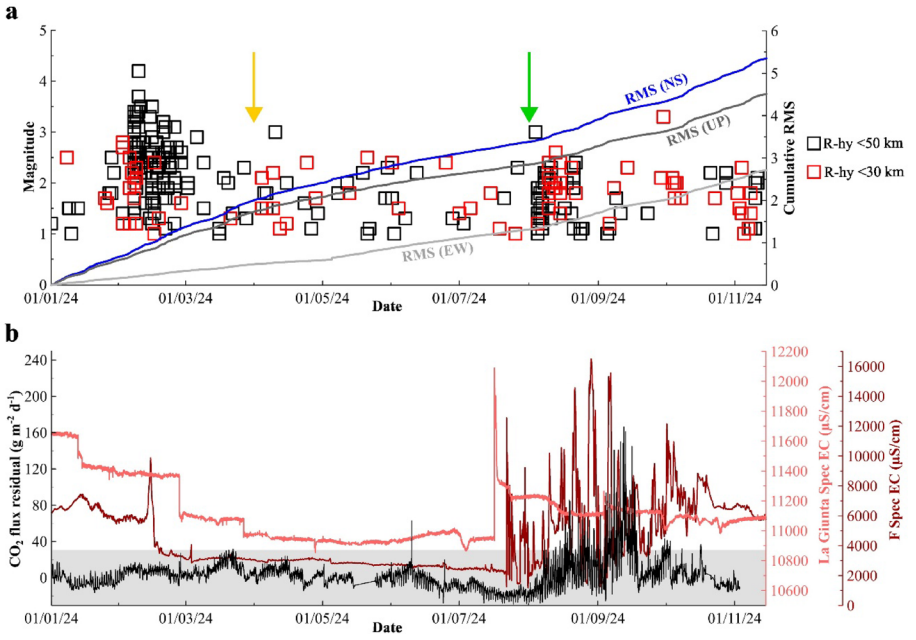

Fig. 4 **a** Seismicity occurring from January to mid-November 2024 in an area with a radius of 50 km with respect to the ZO. PDN10 station (refer to Table S5 for the list of earthquakes). In red the subset of seismicity with maximum radius of 30 km. Light grey, dark grey and blue solid lines indicate the cumulative RMS functions for EW, up and NS components respectively. The yellow and green arrows indicate the two breaks in the slope of RMS functions. **b** Time-series of La Giunta (light red) and F (dark red) mud pool EC and residual signal of soil CO_2 fluxes (black) for the same period. Light grey box is the $\pm 2\sigma$ interval referred to the residual

was installed on June 23, 2023, approximately 300 m southwest of the mud pools. Seismic data acquired by ZO.PDN10 follow international standards defined by the FDSN (https://www.fdsn.org/). Real time continuous data are archived in miniSEED format (http://ds.iris.edu/ds/nodes/dmc/data/formats/miniseed) and distributed through the European Integrated Data Archive (EIDA, https://eida.ingv.it/it/). Daily quality control is performed by the ISMDq system (Massa et al. 2022), and data are automatically integrated into the multiparametric MUDA database (Massa et al. 2024).

The period between January and November 2024 was analyzed for seismicity, as this time frame is free from technical problems with the mud pools probes (Fig. 2) and with the seismic station (in 2023, there was an issue with the East component), thus providing the greatest time-series continuity for all the monitoring instruments. Figure 4a shows seismicity recorded during the aforementioned period within a 50 km radius of the ZO.PDN10 station (311 events, Table S5), along with the cumulative RMS function computed across all three components of motion. Noteworthy, due to the strong attenuation of the bubbling drumbeats of the mud volcanoes, ZO.PDN10 is not able to clearly record the bubbling phenomena, well captured instead by the temporary seismic station installed a few meters away from the mud pools. Focusing on the local and regional seismicity of tectonic origin, the results reveal three distinct seismic phases effectively captured by the fluctuations of the

cumulative RMS functions calculated starting from the continuous data stream recorded at ZO.PDN10:

(1) a high-activity period from January to early March, 2024, associated with a seismic swarm in the northwestern Apennines characterized by more than 200 earthquakes with magnitude ranging from ML 1.5 to Mw 4.2 (i.e. February 9, 2024, 12:06:21 UTC; https://terremoti.ingv.it/en);
(2) a quiescent phase from March to July, with sparse and low-magnitude events;
(3) renewed seismic activity beginning in August, characterized by several clusters including 40 earthquakes with ML ranging from 1.5 to 3.0, within 30 km of ZO.PDN10.

5 Discussion

The time series acquired from the mud pools (Fig. 2a–b) and the soil CO_2 flux station (Fig. 3a) clearly demonstrate that fluid emissions at Salse di Nirano vary over time, displaying both short- and long-term trends, abrupt spikes, gradual shifts and periodic oscillations. These variations reflect the influence of both endogenous and exogenous factors. Disentangling these contributions is essential for identifying changes linked to subsurface dynamics and for assessing possible links with seismicity. In this context, the implementation of a high-frequency, multiparametric monitoring network has proven to be a powerful approach.

5.1 Environmental forcing on mud volcano fluids

Mud pool dynamics show a clear sensitivity to short, intense precipitations, whilst atmospheric pressure does not significantly affect the mud level (Table S2, Fig. S3), in agreement with previous findings at Salse di Nirano by Giambastiani et al. (2022). Mud temperature exhibits a seasonal trend that closely follows air temperature (Fig. 2; Table S2). In contrast, EC shows no consistent correlation with environmental variables, suggesting it is a more direct indicator of subsurface fluid circulation.

Air temperature and humidity likely influence near-surface diffusivity, modulating the CO_2 exchange between soil and atmosphere, as suggested by the diurnal cyclicity common to all three parameters (Fig. 3b–d). Daily biological activity may also play a role in this cycle (Silvola et al. 1985, 1996; Nakadai et al. 2002). The multivariate regression analysis (MRA) revealed a negative correlation between air temperature and CO_2 flux, as observed at other volcanic and hydrothermal systems (Viveiros et al. 2008, 2014, 2015; Carapezza et al. 2009; Camarda et al. 2016, 2019). Rinaldi et al. (2012) attributed this to the density dependence of gas flow: lower air temperatures increase CO_2 density, thus enhancing flux. Soil temperature and humidity also influence fluxes: higher soil temperatures enhance gas agitation and convective transport, while low soil humidity favors permeability by keeping pores free of water. The multivariate regression model explains CO_2 flux variability to a modest extent (~19%). The remaining variations of the residual are likely linked to other unmonitored environmental variables and to endogenous factors, including changeable seismic-related stress-strain conditions.

5.2 Fluid circulation and seismicity link: insights from continuous monitoring

The soil CO_2 flux map from our survey carried out in July 2023 reveals two distinct alignments of anomalous emissions (Fig. 1b). The NE–SW trend corresponds to the orientation of the main mud volcano alignment and reflects the direction of the Apennine belt compression, as previously reported by Sciarra et al. (2019) and Giambastiani et al. (2024). A second NW–SE trend, associated with higher flux values, aligns with both a prominent terrace scarp—sometimes interpreted as a fault (Castaldini et al. 2005)—and the axis of an anticline fold (Bonini 2007). Sites A and B, which recorded the highest emissions, were also identified in previous surveys (Sciarra et al. 2019; Giambastiani et al. 2024), conducted in different years (2015, 2022, respectively) and seasons, supporting the persistence and non-seasonal nature of these anomalies. Our findings reinforce the strong structural control on degassing pathways and the spatial coupling between tectonic features and fluid emissions.

Continuous monitoring of La Giunta and F mud pools from January to November 2024 (Fig. 4b) revealed a parallel evolution in EC, marked by three main events:

(i) a significant decrease in late February (with a transient positive spike at F);
(ii) a stable period from March to early July;
(iii) a sharp increase at the end of July, with variability at F persisting until late October.

These shifts are occasionally accompanied by changes in the mud water level and, more rarely, temperature (Fig. 2a–b). All of them exceed the uncertainty of related sensors (please, refer to Materials and Methods chapter). In addition, these shifts are clearly visible in the first derivative of the cleaned time series (Fig. S6), with rainfall-related spikes removed. Although the timing was nearly simultaneous at both sites (lag of a few days), the magnitude differed significantly: EC changes at F were much larger (~6000 and ~10,000 µS/cm) compared to La Giunta (~230 and ~1140 µS/cm). This suggests a shared deep trigger, likely linked to a change in the feeding system, but modulated by site-specific factors such as ascent paths, variable mixing extent between deep more saline water and shallow meteoric water, permeability contrasts, and the influence of distinct shallow reservoirs (Nespoli et al. 2023; Carfagna et al. 2024; Brindisi et al. 2025).

The EC variability recorded between July and October 2024 coincided with a significant increase in soil CO_2 flux (Figs. 3a, b and 4b), indicating widespread involvement of the fluid system and suggesting a perturbation of the deep plumbing architecture affecting multiple emission sites simultaneously.

To better constrain possible triggers of the observed reservoir changes, we analyzed seismicity within a 50 km radius of Salse di Nirano (Figs. 1a and 4a). Three distinct periods of seismic activity correlate well with the three main EC phases. In particular, the February swarm (Mw 4.2, ~50 km) corresponds to the EC drop in both pools, while the more proximal August swarm (~30 km) is preceded by the pronounced EC increase and is accompanied by a marked rise in soil CO_2 flux. The closer proximity of the August events likely accounts for the stronger system response. Furthermore, the duration of the CO_2 flux anomaly matches that of the EC perturbation observed at F. Conversely, the March–July period of relative seismic quiescence coincides with the stable phase of both mud pools, further supporting the link between deep fluid dynamics and regional seismicity. Weak statistical correlations between the time-series of EC/CO_2 and seismic events were obtained (e.g. Kendall

coefficients ~ 0.1–0.2) and are ascribable to the low number of cases occurring during the analyzed period (only two seismic swarms over almost one year of observations). Longer time-series will provide more reliable statistical data.

6 Conclusions

The results of this study demonstrate the effectiveness of a real-time, high frequency multiparametric monitoring system in capturing complex and dynamic interactions between fluid circulation and seismicity within a tectonically active area characterized by the presence of deep fluids degassing. By integrating geochemical, geophysical, and environmental data from multiple sources, we were able to detect synchronous changes across distinct emission sites and correlate them with episodes of local seismicity. In particular, the observed temporal coincidence between shifts in mud pool electrical conductivity and soil CO_2 degassing with two seismic swarms in 2024 provides compelling evidence that seismic perturbations can modulate the behavior of deep fluid reservoirs and influence surface emissions. Greater statistical significance of the observed phenomena will be possible in the future by continuing this type of monitoring and collecting longer time-series. Moreover, multi-year time-series may help to better understand the relationships between earthquake magnitude, epicentral distance, and mud volcano anomalies.

Our findings suggest that fluid migration and overpressure dynamics, when properly monitored, can serve as valuable indicators of crustal stress changes and potentially precede or respond to seismic activity. Importantly, the persistent CO_2 flux anomalies aligned with tectonic structures reinforce the value of using diffuse degassing surveys to map active faults and preferential pathways for fluid ascent, even in the absence of a seismic crisis.

Furthermore, the multiparametric network deployed at Salse di Nirano sets a benchmark for future multidisciplinary monitoring strategies in similar settings. Its modular and scalable design allows for replication in other tectonically active regions, where fluid-driven processes may influence fault behavior and seismic hazard.

Supplementary Information The online version contains supplementary material available at https://doi.org/10.1007/s11069-026-08071-3.

Acknowledgements We would like to thank the Municipality of Fiorano Modenese (MO) and the Salse di Nirano Nature Reserve, in particular Dr. Marzia Conventi and Luciano Callegari, for authorizing our work in the Nirano mud volcano area, for supporting scientific research, and for providing valuable historical insights into the Salse di Nirano.

Author contributions E.F., A.L.R. and M.M. wrote the original draft. All authors reviewed the manuscript and contributed to the methodological approach of the work and interpretation of data. E.F., G.C.G., A.S., M.M. and S.L. performed the formal analysis.

Funding Open access funding provided by Istituto Nazionale di Geofisica e Vulcanologia within the CRUI-CARE Agreement. This work was supported by the projects INGV Pianeta Dinamico-PROMUD (definition of a multidisciplinary monitoring PROtocol for MUD volcanoes), INGV-DL-50–Task IDRONORD, and PRIN2022HA8XCS.

Declarations

Cnflict of interest The authors have no relevant financial or non-financial interests to disclose.

References

Baciu C, Caracausi A, Etiope G, Italiano F (2007) Mud volcanoes and methane seeps in Romania: main features and gas flux. Ann Geophys-Italy 50(4):501–511

Bonini M (2007) Interrelations of mud volcanism, fluid venting, and thrust-anticline folding: examples from the external northern Apennines (Emilia-Romagna, Italy). J Geophys Res 112:1–21. https://doi.org/10.1029/2006JB004859

Bonini M (2008) Elliptical mud volcano caldera as stress indicator in an active compressional setting (Nirano, Pede-Apennine margin, northern Italy). Geology 36(2):131–134. https://doi.org/10.1130/G24158A

Bonini M (2009) Mud volcano eruptions and earthquakes in the Northern Apennines and Sicily, Italy. Tectonophysics 474:723–735. https://doi.org/10.1016/j.tecto.2009.05.018

Bonini M (2012) Mud volcanoes: Indicators of stress orientation and tectonic controls. Earth Sci Rev 115:121–152. https://doi.org/10.1016/j.earscirev.2012.09.002

Bormann P (2012) New Manual of Seismological Observatory Practice (NMSOP-2), IASPEI, GFZ German Research Centre for Geosciences, Potsdam, Germany, available at http://gfzpublic.gfz-potsdam.de/rest/items/item_152437/component/file_352729/content

Brindisi A, Paolucci E, Carfagna N, Albarello D (2025) Passive seismic measurements to characterize gas reservoirs in a mud volcano field in Northern Italy. Mar Petrol Geol 173:1–8. https://doi.org/10.1016/j.marpetgeo.2024.107275

Camarda M, De Gregorio S, Di Martino RMR, Favara R (2016) Temporal and spatial correlations between soil CO_2 flux and crustal stress. J Geophys Res-Sol Ea 121:7071–7085. https://doi.org/10.1002/2016JB013297

Camarda M, De Gregorio S, Capasso G, Di Martino RMR, Gurrieri S, Prano V (2019) The monitoring of natural soil CO_2 emissions: Issues and perspectives. Earth-Sci Rev 198:102928. https://doi.org/10.1016/j.earscirev.2019.102928

Carapezza ML, Ricci T, Ranaldi M, Tarchini L (2009) Active degassing structures of Stromboli and variations in diffuse CO_2 output related to the volcanic activity. J Volcanol Geoth Res 182:231–245. https://doi.org/10.1016/j.jvolgeores.2008.08.006

Carfagna N, Brindisi A, Paolucci E, Albarello D (2024) Seismic monitoring of gas emissions at mud volcanoes: The case of Nirano (northern Italy). J Volcanol Geoth Res 446:107993. https://doi.org/10.1016/j.jvolgeores.2023.107993

Castaldini D, Coratza P (2017) Mud volcanoes in the Emilia-Romagna Apennines: small landforms of outstanding scenic and scientific value. In: Soldati M, Marchetti M (eds.) Landscapes and Landforms of Italy, Springer International Publishing AG, 225–234. https://doi.org/10.1007/978-3-319-26194-2

Castaldini D, Valdati J, Ilies DC, Chiriac C, Bertogna I (2005) Geo-tourist map of the natural reserve of Salse Di Nirano (Modena Apennines, Northern Italy). Italian J Quaternary Sci 18(1):245–255

Castaldini D, Coratza P, De Nardo MT (2017) Geologia e geomorfologia delle Salse di Nirano. Supplementi degli Atti della Società dei Nat e Matematici di Modena 148:23–58

Chao H-C, You C-F, Sun C-H (2010) Gases in Taiwan mud volcanoes: Chemical composition, methane carbon isotopes, and gas fluxes. Appl Geochem 25:428–436. https://doi.org/10.1016/j.apgeochem.2009.12.009

Chen Z, Li Y, Liu Z, Zheng G, Xu W, Yan W, Yi L (2019) CH4 and CO2 emissions from mud volcanoes on the southern margin of the Junggar Basin, NW China: Origin, output, and relation to regional tectonics. J Geophys Res-Sol Ea 124:5030–5044. https://doi.org/10.1029/2018JB016822

Chiodini G, Cioni R, Guidi M, Raco B, Marini L (1998) Soil CO_2 flux measurements in volcanic and geothermal areas. Appl Geochem 13:543–552

Cipriani A, Lugli F, Martinelli G, Sciarra A (2017) Analisi isotopiche (87Sr/86Sr, δ18O, δD e trizio) delle Salse di Nirano. Supplementi degli Atti della Società dei Nat e Matematici di Modena 148:155–165

Coppi F (1875) Brevi note sulle Salse Modenesi. Bollettino del R Comitato Geol 7–8:1–7

Danecek P, Pintore S, Mazza S, Mandiello A, Fares M, Carluccio I et al (2021) The Italian node of the European integrated data archive. Seismological Soc Am 92:1726–1737. https://doi.org/10.1785/0220200409
Delisle G, Teschner M, Faber E, Panahi B, Guliev I, Aliev C (2011) First approach in quantifying fluctuating gas emissions of methane and radon from mud volcanoes in Azerbaijan. In: Shale Tectonics. Am Association Petroleum Geol. https://doi.org/10.1306/13231316M933426
Deville E, Guerlais S-H (2009) Cyclic activity of mud volcanoes: evidences from Trinidad (SE Caribbean). Mar Petrol Geol 26:1681–1691. https://doi.org/10.1016/j.marpetgeo.2009.03.002
Draper N, Smith H (1981) Applied regression analysis. 2nd edition, John Wiley & Sons, Chichester
Etiope G (2015) Natural gas seepage. The earth's hydrocarbon degassing. Springer International Publishing, Switzerland 199. https://doi.org/10.1007/978-3-319-146010
Etiope G, Martinelli G (2009) Pieve Santo Stefano is not a mud volcano: comment on structural controls on a carbon dioxide-driven mud volcano field in the Northern Apennines (by Bonini, 2009). J Struct Geol 31:1270–1271. https://doi.org/10.1016/j.jsg.2009.06.009
Etiope G, Baciu C, Caracausi A, Italiano F, Cosma F (2004a) Gas flux to the atmosphere from mud volcanoes in eastern Romania. Terra Nova 16:179–184. https://doi.org/10.1111/j.1365-3121.2004.00542.x
Etiope G, Feyzullayev A, Baciu C, Milkov AV (2004b) Methane emission from mud volcanoes in the Eastern Azerbaijan. Geology 32(6):465–468. https://doi.org/10.1130/G20320.1
Etiope G, Martinelli G, Caracausi A, Italiano F (2007) Methane seeps and mud volcanoes in Italy: Gas origin, fractionation and emission to the atmosphere. Geophys Res Lett 34:1–5. https://doi.org/10.1029/2007GL030341
Etiope G, Nakada R, Tanaka K, Yoshida N (2011) Gas seepage from Tokamachi mud volcanoes, onshore Niigata Basin (Japan): Origin, post-genetic alterations and CH_4-CO_2 fluxes. Appl Geochem 26:348–359. https://doi.org/10.1016/j.apgeochem.2010.12.008
Ferrari E, Massa M, Lovati S, Di Michele F, Rizzo AL (2024) Multiparametric stations for real-time monitoring and long-term assessment of natural hazards. Front Earth Sci 12:1412900. https://doi.org/10.3389/feart.2024.1412900
Feseker T, Foucher J-P, Harmegnies F (2008) Fluid flow or mud eruptions? Sediment temperature distributions on Håkon Mosby mud volcano, SW Barents Sea slope. Mar Geol 247:194–207. https://doi.org/10.1016/j.margeo.2007.09.005
Feseker T, Dählmann A, Foucher J-P, Harmegnies F (2009) In-situ sediment temperature measurements and geochemical pore water data suggest highly dynamic fluid flow at Isis mud volcano, eastern Mediterranean Sea. Mar Geol 261:128–137. https://doi.org/10.1016/j.margeo.2008.09.003
Feseker T, Boetius A, Wenzhöfer F, Blandin J, Olu K, Yoerger DR et al (2014) Eruption of a deep-sea mud volcano triggers rapid sediment movement. Nat Commun 5:1–8. https://doi.org/10.1038/ncomms6385
Freund RJ, Wilson WJ (1998) Regression analysis. Statistical modelling of a response variable. Academic, New York
Gasperi G, Bettelli G, Panini F, Pizziolo M, Bonazzi U, Fioroni C et al (2005) Note illustrative della carta geologica d'Italia alla scala 1:50000, foglio 219 Sassuolo. Regione Emilia-Romagna. ISPRA Geological Survey of Italy
Giambastiani BMS, Antonellini M, Nespoli M, Bacchetti M, Calafato A, Conventi M et al (2022) Mud flow dynamics at gas seeps-Nirano Salse, Italy -. Environ Earth Sci 81:480. https://doi.org/10.1007/s12665-022-10615-2
Giambastiani BMS, Chiapponi E, Polo F, Nespoli M, Piombo A, Antonellini M (2024) Structural control on carbon emissions at the Nirano mud volcanoes–Italy. Mar Petrol Geol 163:106771. https://doi.org/10.1016/j.marpetgeo.2024.106771
Goldstein P, Dodge D, Firpo M, Minner L (2003) 85.5 - SAC2000: Signal processing and analysis tools for seismologists and engineers. Int Geophys 81:1613–1614. https://doi.org/10.1016/S0074-6142(03)80284-X
Gorgoni C, Bonori O, Lombardi S, Martinelli G, Sighinolfi GP (1988) Radon and helium anomalies in mud volcanoes from northern Apennines (Italy)-a tool for earthquake prediction. Geochem J 22:265–273
Heller C, Blumenberg M, Kokoschka S, Wrede C, Hoppert M, Taviani M, Reitner J (2011) Geomicrobiology of fluid venting structures at the salse di Nirano mud volcano area in the northern Apennines (Italy). In: Reitner J, (Ed.), Advances in stromatolite geobiology, Lecture Notes in Earth Sciences, 131:209–220. https://doi.org/10.1007/978-3-642-10415-2_14
ITHACA Working Group (2019) ITHACA (ITaly HAzard from CApable faulting), A database of active capable faults of the Italian territory. Version December 2019. ISPRA Geological Survey of Italy. Web Portal http://sgi2.isprambiente.it/ithacaweb/Mappatura.aspx
Kaul N, Foucher J-P, Heesemann M (2006) Estimating mud expulsion rates from temperature measurements on Håkon Mosby Mud Volcano, SW Barents Sea. Mar Geol 229:1–14. https://doi.org/10.1016/j.margeo.2006.02.004

Kopf A, Delisle G, Faber E, Panahi B, Aliyev CS, Guliyev I (2010) Long-term in situ monitoring at Dashgil mud volcano, Azerbaijan: a link between seismicity, pore-pressure transients and methane emission. Int J Earth Sci 99(1):227–240. https://doi.org/10.1007/s00531-009-0487-4

Lucian G, Vallocchia M, Antunes V, Lupi M, Obermann A, Mazzini A et al (2017) Esperimento di sismica passiva per lo studio di dettaglio dei vulcani di fango nella riserva naturale regionale delle Salse di Nirano (Modena). Rapporti tecnici INGV, numero 382

Lupi M, Ricci BS, Kenkel J, Ricci T, Fuchs F, Miller SA, Kemna A (2016) Subsurface fluid distribution and possible seismic precursory signal at the Salse di Nirano mud volcanic field, Italy. Geophys J Int 204(2):907–917. https://doi.org/10.1093/gji/ggv454

Luzi L, Pacor F, Ameri G, Puglia R, Burrato P, Massa M et al (2013) Overview on the strong-motion data recorded during the May–June 2012 Emilia seismic sequence. Seismol Res Lett 84(4):629–644. https://doi.org/10.1785/0220120154

Manga M, Brumm M, Rudolph ML (2009) Earthquake triggering of mud volcanoes. Mar Petrol Geol 26:1785–1798. https://doi.org/10.1016/j.marpetgeo.2009.01.019

Martinelli G, Dadomo A (2005) Mud volcano monitoring and seismic events. In: Martinelli G, Panahi B (eds) Mud Volcanoes, Geodynamics and Seismicity. NATO Science Series, vol 51. Springer, Dordrecht. doi:https://doi.org/10.1007/1-4020-3204-8_17

Martinelli G, Dadomo A (2017) Misura in continuo di temperatura e livello del fango in una emissione selezionata delle Salse di Nirano. Supplementi degli Atti della Società dei Nat e Matematici di Modena 148:99–104

Martinelli G, Ferrari G (1991) Earthquake forerunners in a selected area of Northern Italy: recent developments in automatic geochemical monitoring. Tectonophysics 193(4):397–410. https://doi.org/10.1016/0040-1951(91)90348-V

Martinelli G, Albarello D, Mucciarelli M (1995) Radon emissions from mud volcanoes in Northern Italy: possible connection with local seismicity. Geophys Res Lett 22(15):1989–1992. https://doi.org/10.1029/95GL01785

Massa M, Scafidi D, Mascandola C, Lorenzetti A (2022) Introducing ISMDq-A web portal for real-time quality monitoring of Italian strong-motion data. Seismol Res Lett 93(1):241–256. https://doi.org/10.1785/0220210178

Massa M, Rizzo AL, Scafidi D, Ferrari E, Lovati S, Luzi L, MUDA working group (2024) MUDA: dynamic geophysical and geochemical MUltiparametric DAtabase. Earth Syst Sci Data 16:4843–4867. https://doi.org/10.5194/essd-16-4843-2024

Mazzini A, Etiope G (2017) Mud volcanism: an updated review. Earth-Sci Rev 168:81–112. https://doi.org/10.1016/j.earscirev.2017.03.001

Mellors R, Kilb D, Aliyev A, Gasanov A, Yetirmishli G (2007) Correlations between earthquakes and large mud volcano eruptions. J Geophys Res 112:B04304. https://doi.org/10.1029/2006JB004489

Milkov AV, Etiope G (2018) Revised genetic diagrams for natural gases based on a global dataset of > 20,000 samples. Org Geochem 125:109–120. https://doi.org/10.1016/j.orggeochem.2018.09.002

Minissale A, Magro G, Martinelli G, Vaselli O, Tassi GF (2000) Fluid geochemical transect in the Northern Apennines (central-northern Italy): Fluid genesis and migration and tectonic implications. Tectonophysics 319:199–222. https://doi.org/10.1016/S0040-1951(00)00031-7

MPS Working Group (2004) Redazione della mappa di pericolosità sismica prevista dall'Ordinanza PCM del 20 marzo 2003. Rapporto Conclusivo per il Dipartimento della Protezione Civile

Nakadai T, Yokozawa M, Ikeda H, Koizumi H (2002) Diurnal changes of carbon dioxide flux from brownfield in agricultural field in Japan. Appl Soil Ecol 19(2):161–171. https://doi.org/10.1007/s00704-004-0094-z

Nespoli M, Antonellini M, Albarello D, Lupi M, Cenni N, Piombo A (2023) Gravity data allow to image the shallow-medium subsurface below mud volcanoes. Geophys Res Lett 50:e2023GL103505. https://doi.org/10.1029/2023GL103505

Oliveira S, Viveiros F, Silva C, Pacheco JE (2018) Automatic filtering of soil CO_2 flux data; different statistical approaches applied to long time series. Front Earth Sci 6:208. https://doi.org/10.3389/feart.2018.00208

Oppo D, Capozzi R, Picotti V (2013) A new model of the petroleum system in the Northern Apennines, Italy. Mar Petrol Geol 48:57–76. https://doi.org/10.1016/j.marpetgeo.2013.06.005

Queißer M, Burton MR, Arzilli F, Chiarugi A, Marliyani GI, Anggara F, Harijoko A (2017) CO_2 flux from Javanese mud volcanism. J Geophys Res-Sol Ea 122:4191–4207. https://doi.org/10.1002/2017JB013968

Raich JW, Tufekcioglu A (2000) Vegetation and soil respiration: correlations and controls. Biogeochemistry 48(1):71–90

Rao S, Salvaterra L, Acerra C (2010) Software per l'installazione e la configurazione della stazione sismica GAIA2. Rapporti Tecnici INGV 130:52

Rinaldi AP, Vandemeulebrouck J, Todesco M, Viveiros F (2012) Effects of atmospheric conditions on surface diffuse degassing. J Geophys Res 117:B11201. https://doi.org/10.1029/2012JB009490

Rovida A, Locati M, Camassi R, Lolli B, Gasperini P (2020) The Italian earthquake catalogue CPTI15. B Earthq Eng 18:2953–2984. https://doi.org/10.1007/s10518-020-00818-y

Sciarra A, Cantucci B, Ricci T, Tomonaga Y, Mazzini A (2019) Geochemical characterization of the Nirano mud volcano, Italy. Appl Geochem 102:77–87. https://doi.org/10.1016/j.apgeochem.2019.01.006

Silvola J, Välijoki J, Aaltonen H (1985) Effect of draining and fertilization on soil respiration at three ameliorated peatland sites. Acta Forestalia Fennica 191:1–32

Silvola J, Alm J, Ahlholm U, Nykänen H, Martikainen PJ (1996) CO_2 fluxes from peat in boreal mires under varying temperature and moisture conditions. J Ecol 84:219–228

Sinclair AJ (1974) Selection of threshold values in geochemical data using probability graphs. J Geochem Explor 3:129–149

Stucchi M, Meletti C, Montaldo V, Crowley H, Calvi GM, Boschi E (2011) Seismic hazard assessment (2003–2009) for the Italian building code. B Seismol Soc Am 101:1885–1911. https://doi.org/10.1785/0120100130

Tassi F, Bonini M, Montegrossi G, Capecchiacci F, Capaccioni B, Vaselli O (2012) Origin of light hydrocarbons in gases from mud volcanoes and CH4-rich emissions. Chem Geol 294–295:113–126. https://doi.org/10.1016/j.chemgeo.2011.12.004

Van Camp M, Vauterin P (2005) Tsoft: graphical and interactive software for the analysis of time series and Earth tides. Comput Geosci 31(5):631–640. https://doi.org/10.1016/j.cageo.2004.11.015

Viveiros F, Ferreira T, Cabral Vieira J, Silva C, Gaspar JL (2008) Environmental influences on soil CO_2 degassing at Furnas and Fogo volcanoes (São Miguel Island, Azores archipelago). J Volcanol Geoth Res 177:883–893. https://doi.org/10.1016/j.jvolgeores.2008.07.005

Viveiros F, Vandemeulebrouck J, Rinaldi P, Ferreira T, Silva C, Cruz JV (2014) Periodic behavior of soil CO_2 emissions in diffuse degassing areas of the Azores archipelago: application to seismovolcanic monitoring. J Geophys Res-Sol Ea 119:7578–7597. https://doi.org/10.1002/2014JB011118

Viveiros F, Ferreira T, Silva C, Vieira JC, Gaspar JL, Virgili G, Amaral P (2015) Permanent monitoring of soil CO_2 degassing at Furnas and Fogo volcanoes (São Miguel Island, Azores). In: Gaspar J L, Guest J E, Duncan A M, Barriga F J A S, Chester D K (eds), Volcanic Geology of São Miguel Island (Azores Archipelago), Geological Society, London, Memoirs 44:271–288. https://doi.org/10.1144/M44.20

Yang TF, Yeh G-H, Fu C-C, Wang C-C, Lan T-F, Lee H-F et al (2004) Composition and exhalation flux of gases from mud volcanoes in Taiwan. Environ Geol 46:1003–1011. https://doi.org/10.1007/s00254-004-1086-0